

Extended homologous series of Sn-O layered systems: a first-principles study

Kirsten Govaerts,¹ Bart Partoens,² and Dirk Lamoen^{1,*}

¹*EMAT, Department of Physics, Universiteit Antwerpen,
Groenenborgerlaan 171, 2020 Antwerpen, Belgium*

²*CMT group, Department of Physics, Universiteit Antwerpen,
Groenenborgerlaan 171, 2020 Antwerpen, Belgium*

Abstract

Apart from the most studied tin-oxide compounds, SnO and SnO₂, intermediate states have been claimed to exist for more than a hundred years. In addition to the known homologous series (Seko et al., Phys. Rev. Lett. 100, 045702 (2008)), we here predict the existence of several new compounds with an O concentration between 50 % (SnO) and 67 % (SnO₂). All these intermediate compounds are constructed from removing one or more (101) oxygen layers of SnO₂. Since the van der Waals (vdW) interaction is known to be important for the Sn-Sn interlayer distances, we use a vdW-corrected functional, and compare these results with results obtained with PBE and hybrid functionals. We present the electronic properties of the intermediate structures and we observe a decrease of the band gap when (i) the O concentration increases and (ii) more SnO-like units are present for a given concentration. The contribution of the different atoms to the valence and conduction band is also investigated.

Keywords: A. Semiconductors; C. Density Functional Theory; C. van der Waals functional; A. Layered structures

I. INTRODUCTION

SnO₂ and SnO are the most studied tin-oxide compounds, showing a wide variety of technological applications. The former is most known as an opacifier of glazes¹, it can also be used as a polishing powder², it can help to adhere a protective polymer coating³ and it acts as a functional material for solar cells⁴, transparent conducting oxides^{5,6} and gas sensors⁷. SnO is used for the production of tin salts for electroplating⁸ and is known as an anode material for Li-rechargeable batteries⁹. Moreover SnO is a good p-type semiconductor¹⁰, which can even be converted from p- to n-type after doping with Sb¹¹.

Both SnO₂ and SnO have a tetragonal structure in their most stable form. For SnO₂ this is the rutile structure (space group $P4_2/mnm$) with lattice parameters $a = 4.7374 \text{ \AA}$ and $c = 3.1864 \text{ \AA}$. In Fig. 1 (a) it can be seen that SnO₂ has two formula units per unit cell and an internal parameter, $u = 0.30562$, fixing the positions of the O atoms¹². The most stable form of SnO is the so-called litharge structure (space group $P4/nmm$) with lattice parameters $a = 3.8011 \text{ \AA}$, $c = 4.8352 \text{ \AA}$. In Fig. 1 (b) it can be seen that also SnO has two formula units per unit cell with internal parameter, $u = 0.23818$ ¹³, fixing the positions of the Sn atoms located at the apex of the square pyramid with a base of O atoms. This results in a layered stacking of Sn-O-Sn slabs along the [001] direction with each slab consisting of an oxygen layer sandwiched between two tin layers. Between the Sn-O-Sn slabs i.e. between adjacent Sn layers a weak van der Waals (vdW) bonding exists with a distance of 2.53 \AA between successive slabs.

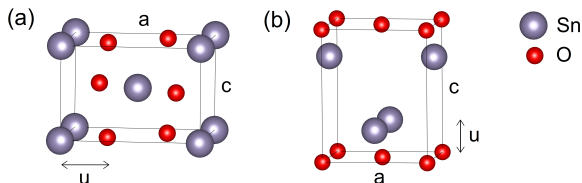


Figure 1: Unit cells of (a) SnO₂ and (b) SnO.

Apart from these well-known compounds, intermediate states have been claimed to exist for more than a hundred years. Many phase diagrams have already been proposed in literature, but they do not agree with each other¹⁴. The intermediate states arise in the disproportionation of SnO at higher temperatures: apart from the (usually wanted) end products SnO₂ and Sn, also (usually unwanted) intermediate oxides occur. Additionally,

SnO₂ often shows oxygen deficiency, which plays a central role in determining properties and chemical activities. Recently it was shown that a Sn₂O₃-based NO gas sensor demonstrated an improved selectivity to NO, NO₂, and CO gases¹⁵. Another study remarks the presence of Sn₃O₄ in ultrathin SnO₂ nanosheets, which show superior performance for lithium-ion storage¹⁶. The compounds Sn₃O₄^{14,17-23}, Sn₂O₃^{24,25} and to a lesser extent Sn₅O₆²⁶, have already been the subject of research.

Based on a cluster expansion (CE) in combination with simulated annealing, Seko et al.²⁷ suggested the existence of a homologous series Sn_{*n*+1}O_{2*n*} of (meta)stable compounds. These structures have oxygen vacancies layered on (101) planes of the rutile lattice of SnO₂, as shown in Fig. 2 for Sn₃O₄ and Sn₂O₃ structures. For the latter, this was already observed in Ref. 28 where different possible structures were investigated with ab initio techniques, resulting in a lowest energy for the structure with oxygen vacancies layered on the (101) planes of SnO₂.

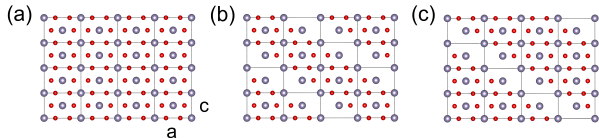


Figure 2: Crystal structures of (a) SnO₂, (b) Sn₃O₄ and (c) Sn₂O₃.

Data concerning the stability and the details of the crystal structures of the intermediate compounds, however, is very rare. The foregoing results have motivated us to search for new Sn-O compounds and to investigate their stability and electronic properties.

In this study we investigate first the stability of different proposed Sn-O structures from the known homologous series Sn_{*n*+1}O_{2*n*} with *n* = 2, 3, 4, 5, 6. When relaxing these structures, we start from a SnO₂ superstructure and remove one oxygen layer, resulting in unit cells consisting of two formula units. This can be seen in the upper part of Fig. 3, where in structure (a), the removed O layer is shown by the light atoms. In the following we will refer to these structures as series A. In addition to this homologous series Sn_{*n*+1}O_{2*n*} we also removed two non-successive O layers, resulting in the structures shown in the lower part of Fig. 3. For structures (f)-(h), this results in a small unit with only one O layer in between two Sn layers - further referred to as SnO unit - and a larger building block of series A, (a)-(c) respectively. We will refer to these structures as series B. In structure (i) we also removed two O layers, now resulting in a unit cell consisting of two building blocks of series

A, (a) and (b). The structures (f)-(i) are not mentioned by Seko et al. but can also be described by a homologous series $\text{Sn}_{n+2}\text{O}_{2n}$ and the unit cells again consist of two formula units. We investigate their stability and compare this with the stability of the homologous series $\text{Sn}_{n+1}\text{O}_{2n}$, i.e. series A.

In Ref. 29 it was shown that the vdW interaction is important between two adjacent Sn-layers. Therefore we compare the stability of the intermediate Sn-O structures obtained by relaxing them with and without the use of a vdW-corrected functional. In a second part of this study the structural properties of the structures are investigated using different exchange- and correlation (xc) functionals: a generalized gradient approximation, a vdW-corrected density functional and a hybrid functional. We relax both the lattice parameters and the atomic positions with the three functionals. Furthermore we discuss the electronic properties of these structures. Whereas the structural properties can be understood from the extreme cases of SnO and SnO_2 , the resulting electronic properties are not straightforward.

II. COMPUTATIONAL DETAILS

The Vienna *ab initio* simulation package VASP^{30,31} was used to optimize lattice parameters and atomic positions. We used the all-electron projector augmented wave (PAW) method with the Sn ($5s^25p^24d^{10}$) and O ($2s^22p^4$) electrons treated as valence electrons. For the xc functional we considered both the generalized gradient approximation of Perdew-Burke-Ernzerhof (PBE)³², the vdW-DF, optB86b, discussed in ref.³³, and the hybrid functional proposed by Heyd, Scuseria and Ernzerhof (HSE06) using a mixing parameter $\alpha = 0.25$ ^{34,35}.

For total energy calculations and structure optimization we used a Γ -centered Monkhorst-Pack k -points grid³⁶ for the Brillouin zone integration. For the PBE and vdW calculations, the plane wave cutoff value was 800 eV, and for the HSE 600 eV. The total number of k -points was chosen so that our results are converged within 10^{-4} eV/atom. The results were considered converged when the energy difference between two successive steps was smaller than 10^{-5} eV and for the geometry optimization we considered a convergence criterium for the forces on the atoms of less than 10^{-3} eV/Å for the PBE and vdW calculations, and $5 \cdot 10^{-3}$ eV/Å for the HSE calculation.

Only for SnO and SnO_2 we performed G_0W_0 calculations^{37,38}, where we used a $6 \times 6 \times 6$

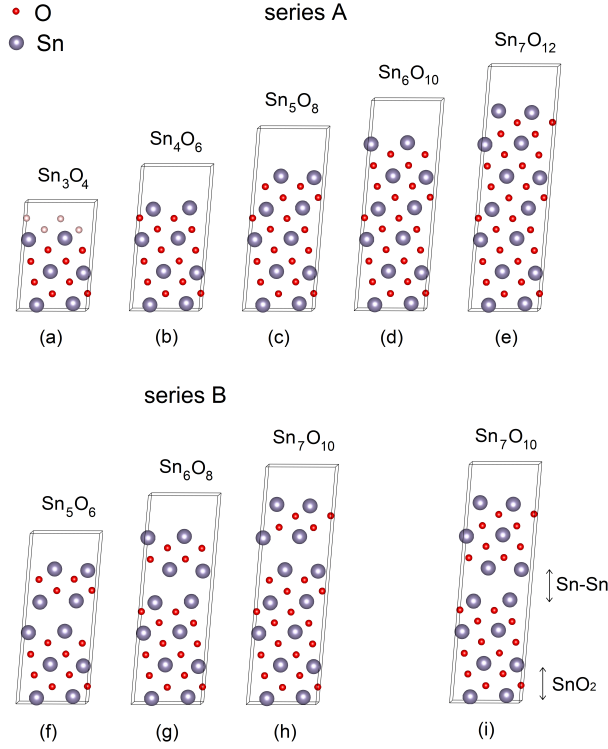


Figure 3: The unit cells of nine different structures, resulting from removing one or more oxygen layers on (101) planes from the SnO_2 structure. In structure (a) the removed oxygen layer is shown by the light atoms. The structures of series A - structures (a)-(e) - are elements of the homologous series $\text{Sn}_{n+1}\text{O}_{2n}$ with $n = 2, 3, 4, 5, 6$ respectively. Structures (f)-(i) are new, where structures (f)-(h) - series B - exhibit a small unit of an oxygen layer in between two Sn layers (i.e. SnO unit), structure (i) is composed of two structures of series A. Each unit cell consists of two formula units. In structure (i), the Sn-Sn interlayer distance and the thickness of the SnO_2 unit are denoted by arrows.

and $4 \times 4 \times 6$ k -point grid respectively, 80 empty bands and a cutoff energy of 600 eV.

III. RESULTS

A. Energetic stability

The nine structures of Fig. 3 are the compounds with the smallest unit cells with a composition between SnO and SnO_2 , that can be formed when removing one or two O layers from a SnO_2 structure. In Ref. 29 it was shown that the vdW interaction plays

an important role in the SnO structure, particularly between adjacent Sn layers. In the intermediate Sn-O structures, the O layers between two Sn layers are removed, resulting in adjacent Sn layers, where we expect the vdW interaction to be non negligible.

To investigate this effect, we relax the structures with the regular PBE functional and with the optB86b-vdW functional. Formation energies - with respect to O₂ and elemental Sn - of all structures with these two functionals are shown in Fig. 4 (a) and (b) respectively, for O concentration ranging from 50 % (i.e. SnO) to 66 % (i.e. SnO₂). For the PBE-relaxed structures the convex hull of these formation energies is similar to the one of Seko et al²⁷. Structures of series A are found to be ground state structures. The convex hull of the vdW-relaxed structures however, shows that these structures are all slightly above the convex hull (2-5 meV/atom), and should therefore be considered as metastable structures. However, in principle entropic effects can stabilize these structures at finite temperature and in any case the energy difference of these metastable structures with the convex hull is small enough to be observed experimentally³⁹. One should also keep in mind that vdW-DFs have been tested less in comparison with the standard PBE functional when it comes to the accurate prediction of ground state energies. We also relaxed the structures using a hybrid functional, and their stability is similar to the PBE-relaxed structures.

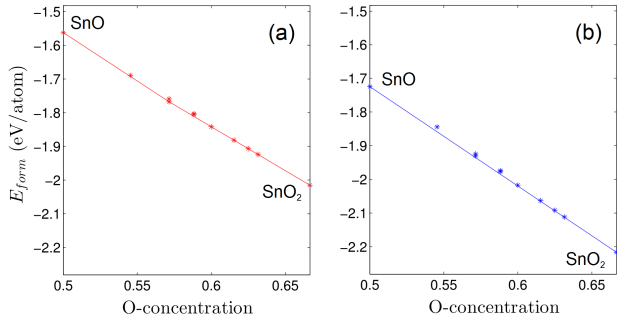


Figure 4: Convex hull of Sn-O structures relaxed with (a) PBE and (b) optB86b-vdW.

In addition to the homologous series Sn_{n+1}O_{2n} (series A) we considered structures from the homologous series Sn_{n+2}O_{2n} (series B and structure (i) of Fig. 3). These structures are metastable at T = 0 K because their formation energy is slightly above the convex hull (2-7 meV/atom), both for the PBE- and vdW-relaxed structures. Again we would like to emphasize that such small energy differences could very well be compensated at elevated temperatures by entropic effects³⁹. Structures of series B are composed of a larger building

block of series A, and one small SnO unit, while structure (i) is composed of two building blocks of series A. Structures (h) and (i) have the same composition, but O layers are removed at different places, resulting in structures composed of different building blocks. From the formation energies of these structures we conclude that structure (i) is favored by 2.6 meV/atom. This means that the Sn-O compounds favor the formation of larger building blocks.

If we remove more O layers resulting in a structure with 50 % O, it did not relax to the SnO ground state structure. It is trapped in a local minimum, which differs by 6.3 meV/atom from the stable litharge structure of SnO. In the following, when SnO is mentioned, one should keep in mind that we refer to its stable litharge ground state structure.

B. Structural properties

When discussing the structural properties of the intermediate Sn-O structures, we compare the two most relevant features: the Sn-Sn interlayer distance and the thickness of the SnO₂ unit, from which the structures are built up. These two features are shown in Fig. 3 (i). Besides using PBE and optB86b-vdW functionals, we also relaxed the structures using the HSE06 hybrid functional.

In Ref. 29, the Sn-Sn interlayer distance of SnO was investigated. As mentioned before, the SnO ground state structure can not be obtained by removing O layers from the SnO₂ structure. In Fig. 5 it is shown that the ordering of Sn atoms in the layers of SnO and the intermediate structures is clearly different. Fig. 5 (a) shows a top view of the adjacent Sn-layers of SnO, while Fig. 5 (b) shows the top view of the adjacent Sn-layers of a typical member of the homologous series, Sn₃O₄. Since this ordering of Sn atoms in the layers is different, interlayer distances will be different.

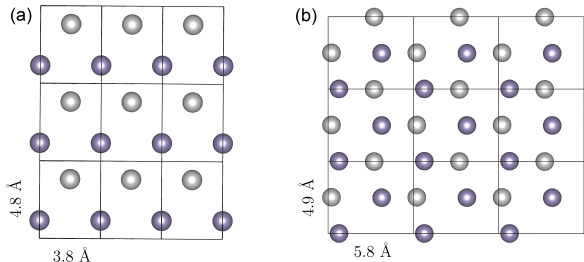


Figure 5: Top view of the two adjacent Sn layers (light and dark atoms) for (a) SnO and (b) Sn₃O₄.

For the Sn-Sn interlayer distance of SnO, the optB86b-vdW functional gives results which are in very good agreement with experiment, as shown in Table I. PBE and HSE overestimate the interlayer distance, although HSE is somewhat better.

Similar results are obtained for the intermediate structures, of which the Sn-Sn interlayer distances are shown in Table I. When comparing the results for the different functionals, the analogy to SnO is clear: PBE leads to the largest values, while the hybrid functional leads to smaller ones. vdW yields the smallest Sn-Sn interlayer distances. We also observe smaller Sn-Sn interlayer distances for the structures of series B. Structure (i), where two O layers are removed resulting in a structure consisting of building blocks of Sn₃O₄ and Sn₄O₆ has a Sn-Sn interlayer distance in between that of Sn₃O₄ and Sn₄O₆.

	PBE	vdW	hybrid	exp
SnO	2.705	2.492	2.640	2.533
(a)- (e)+(i)	3.05-3.1	2.81-2.82	2.97-3.00	/
(f)-(h)	3.02-3.05	2.78-2.79	2.94-2.97	/

Table I: Sn-Sn interlayer distances of SnO and the different structures of Fig. 3 (in Å).

We can also compare the thickness of the SnO₂ unit. In Table II this thickness is shown for SnO₂, relaxed with different functionals, and compared with the experimental value. The different values do not differ as much as in the case of SnO, and are all pretty close to the experimental value. All functionals slightly overestimate the SnO₂ thickness, but the value obtained with the hybrid functional is closest to the experimental value.

The same trend can also be seen in the Sn-O structures of Fig. 3, for which the results are shown in Table II. The hybrid functional gives smaller values for the thickness of the SnO₂ unit than the vdW and PBE functionals. The values obtained with the vdW functional are again almost similar for all structures, while the PBE functional gives values of 2.65 Å for the structure with the smallest concentration of O, and 2.69 Å for the structure with the largest O concentration. In particular, when the O concentration is smaller than 60 %, the vdW-value is larger than the PBE-value, and when the O concentration exceeds 60 %, the PBE-value gets larger. Also the values obtained with the hybrid functional increase with increasing O concentration. Finally we remark that the thicknesses of SnO₂ units of

structures (f)-(h) are comparable with those of their corresponding SnO₂ units of structures (a)-(c) respectively.

	PBE	vdW	hybrid	exp
SnO ₂	2.693	2.681	2.651	2.643
(a)-(i)	2.65-2.69	2.67-2.68	2.63-2.65	/

Table II: Thickness of SnO₂ building block of SnO₂ and the different structures of Fig. 3 (in Å).

C. Electronic properties

Before looking at the band gap of the intermediate structures, we present the results for the two known compounds SnO and SnO₂ in Table III. The band gap calculated with PBE, vdW and hybrid functionals belong to the structures relaxed with these respective functionals. The band gap of the structure relaxed with the vdW functional, is also calculated within the G_0W_0 approximation.

	PBE	vdW	hybrid	G_0W_0	exp
SnO	0.43	0.16	0.59	0.60	0.7
SnO ₂	0.66	0.84	2.95	2.49	3.6

Table III: Band gap (in eV) of SnO and SnO₂ for different functionals.

In the case of SnO, G_0W_0 gives a band gap in very good agreement with the experiment, however the value obtained with the hybrid functional is also close to the experimental value. In the case of SnO₂ the hybrid functional clearly gives the best result. We should remark that the G_0W_0 results strongly depend on the starting wave functions, and here we used starting wave functions from a PBE calculation. Since structural differences are small when SnO₂ is relaxed using the different functionals, the difference in band gap is mainly due to changes in the electron density as a result of the different functionals. This is not the case for SnO, where not only the use of a specific functional for calculating the band gap, but also the large differences in structural parameters - arising when relaxing with the different functionals - cause differences in the band gap.

Whereas for SnO, the vdW gap is smaller than the PBE gap, the opposite is true for SnO₂. Therefore one expects a transition somewhere in between. Figure 6 shows the band gap for all structures, calculated with the different functionals. For the structures with an O concentration smaller than 58 %, PBE gives indeed a larger band gap than the vdW-DF. The vdW and PBE calculated band gap do not differ much, while the hybrid functional opens the gap with ~ 1 eV. The band gap of the structures of series A monotonically decrease with an increasing O concentration. The same trend can be observed for the band gap of the structures of series B. Structures (a) and (g) have the same concentration but whereas in (a) only one O layer is removed from the initial SnO₂ superstructures, in (g) two O layers are removed, resulting in an additional SnO unit, which makes the band gap decrease by 0.5-0.7 eV. The same decrease of the band gap can be observed for structures (h) and (i), which are both a result of removing two O layers from the SnO₂ structure, but whereas for structure (h) this results in a building block of series A and a small SnO unit, for (i) it results in two building blocks of series A. Therefore we can conclude that the decrease of the band gap is not a result of removing more O layers, but is mainly due to the existence of this small SnO unit in the structure.

Since the hybrid functional underestimates the band gap of SnO and SnO₂ by 15-17 %, one can expect that the band gap of the intermediate compounds calculated with the hybrid functional will also be underestimated by the same amount. There are no experimental (or theoretical) results available to compare with.

Although the band gap decreases monotonically with increasing O concentration, it increases again for SnO₂. In particular for the HSE calculations a steep increase is observed in going from Sn₇O₁₂ (e) to SnO₂.

In Fig. 7 (a) and (b) the band structure of series A and series B, calculated with the vdW-DF, is shown respectively. For both figures, one can see the decrease of the band gap with increasing O concentration.

To gain more insight in the previous findings and confirm earlier claims, we have investigated the contribution of the different atoms to the valence and conduction bands, by calculating the projected DOS. In Fig. 8 we show the DOS of Sn₃O₄ together with its PDOS. The top of the valence band consists of ~ 47 % O-p, ~ 35 % Sn-s and ~ 17 % Sn-p states. These results are similar for the other intermediate structures and is in line with previous studies on the PDOS of SnO^{29,40}. The main contribution for the valence band of SnO₂ is

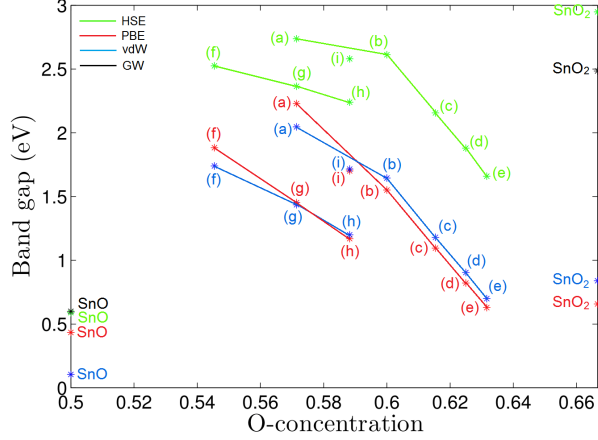


Figure 6: Band gap of all Sn-O structures of Fig. 3, calculated with the PBE (red), optB86b-vdW (blue) and HSE06 (green) functionals. SnO and SnO₂ band gaps are also calculated within the G_0W_0 approximation, on top of the vdW calculation (black).

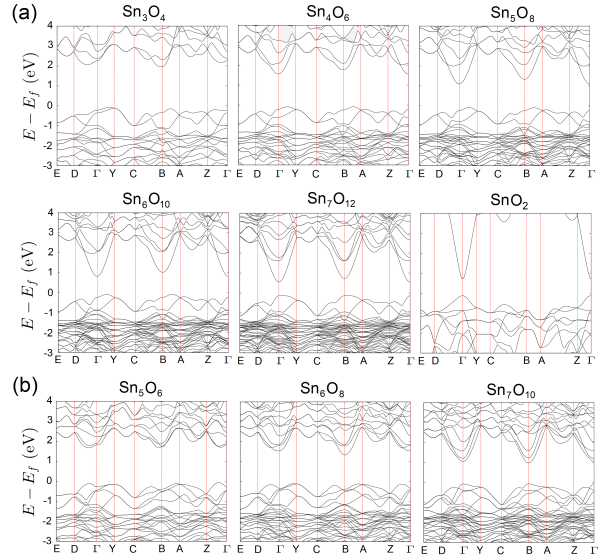


Figure 7: Band structure of structures of (a) series A, and in addition SnO₂, and (b) series B.

O-p, as can be clearly seen in Fig. 9. These findings suggest that the valence band of the intermediate structures is rather similar to the valence band of SnO.

In Fig. 10 (a) the contribution of the Sn atoms next to the removed O layer is shown, i.e. the SnO-like Sn atoms, and Fig. 10 (b) shows the contribution of the Sn atoms which are still in between two O layers, i.e. the SnO₂-like Sn atoms. The valence band is mainly composed of SnO-like Sn atoms, confirming our previous result that the valence band of the intermediate structures is similar to the valence band of SnO.

The conduction band of Sn_3O_4 is a hybridization of SnO-like Sn-p, O-p and SnO_2 -like Sn-s states. When the O concentration increases, the conduction band minimum decreases - leading to a smaller band gap, and these parabolic-shaped bands mainly consist of SnO_2 -like Sn-s and O-p states, which are also the main contribution in the conduction band of SnO_2 , which is shown in Fig. 9.

Since both in conduction and valence band the contribution of SnO-like Sn-atoms is significant, a larger band gap for SnO_2 is reasonable, since it does not have SnO-like Sn atoms. This is in line with the steep increase of the band gap for SnO_2 , calculated with HSE, in Fig. 6.

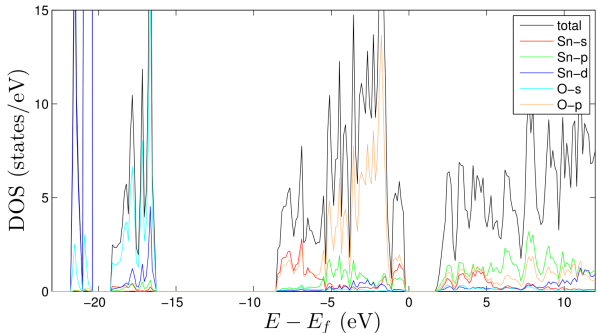


Figure 8: Density of states of Sn_3O_4 . Black lines correspond to the total DOS, colored lines correspond to the projected DOS, as described in the legend.

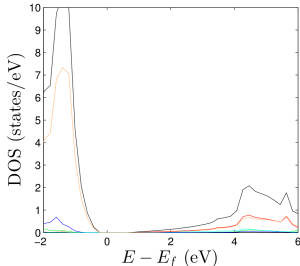


Figure 9: Density of states of SnO_2 around the band gap. The meaning of the colors is the same as in Fig. 8.

IV. CONCLUSION

In this study, we have investigated the stability, structural and electronic properties of Sn-O compounds with an O concentration between 50 % (SnO) and 67 % (SnO_2). Seko

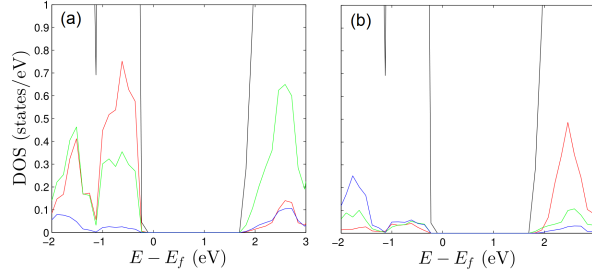


Figure 10: Density of states of Sn_3O_4 around the band gap. Projected DOS of the (a) SnO-like Sn atoms and (b) SnO_2 -like Sn atoms. The meaning of the colors is the same as in Fig. 8.

et al.²⁷ already suggested a homologous series of (meta)stable compounds, with formula $\text{Sn}_{n+1}\text{O}_{2n}$, using ab initio calculations based on the PBE functional. These structures have oxygen vacancies layered on (101) planes of the rutile lattice of SnO_2 . In addition to this homologous series, we have found new (meta)stable structures, arising from removing more than one O layer of SnO_2 .

In addition to PBE calculations we also considered a vdW-corrected functional in order to better describe the Sn-Sn interlayer distances. In contrast to PBE the vdW functional suggests the $\text{Sn}_{n+1}\text{O}_{2n}$ compounds to be metastable rather than stable. Besides PBE and the vdW-corrected functional, the HSE functional was used. We have presented for the first time the electronic properties of the intermediate structures for which we observe a decrease of the band gap when (i) the O concentration increases and (ii) more O layers are removed for a given concentration. Both the valence and the conduction band show a significant contribution of SnO-like Sn-atoms and when the O-concentration increases, the SnO_2 -like Sn-atoms start to dominate the conduction band.

Based on the results of this study we expect that other homologous series of Sn-O structures might be (meta)stable, namely by removing three or more (non-successive) O layers of the SnO_2 superstructure, leading to a compound with a composition given by $\text{Sn}_{n+m}\text{O}_{2n}$ ($n = 2, 3, \dots$, $m = 1, 2, \dots$ and $m < n$).

V. ACKNOWLEDGMENTS

We gratefully acknowledge financial support from a GOA fund of the University of Antwerp. K.G. thanks the University of Antwerp for a PhD fellowship. The computational

resources and services used in this work were provided by the VSC (Flemish Supercomputer Center) and the HPC infrastructure of the University of Antwerp (CalcUA), both funded by the Hercules Foundation and the Flemish Government - department EWI.

- * Electronic address: Dirk.Lamoen@uantwerpen.be
- ¹ A. B. Searle. *The Glazer's Book*. London : The Technical Press, 1935.
 - ² A. F. Holleman and E. Wiberg. *Inorganic Chemistry*. Academic Press, 2001.
 - ³ A. Earnshaw and N. Greenwood. *Chemistry of the Element*. Pergamon Press, 1984.
 - ⁴ S. Franz, G. Kent, and R. L. Anderson. *J. Electron Mater.*, 6:107, 1977.
 - ⁵ M. Batzill and U. Diebold. *Prog. Surf. Sci.*, 79:47, 2005.
 - ⁶ E. Fortunato, D. Ginley, H. Hosono, and D. C. Paine. *Mater. Res. Bull.*, 32:242, 2007.
 - ⁷ W. Göpel and K. .D. Schierbaum. *Sensor Actuat B*, 26:1, 1995.
 - ⁸ Z. Han, N. Guo, F. Li, W. Zhang, H. Zhao, and Y. Qian. *Mater. Lett.*, 48:99, 2001.
 - ⁹ Y. Idota, T. Kubota, A. Matsufuji, Y. Mackawa, and T. Miyasaka. *Science*, 176:1395, 1997.
 - ¹⁰ Y. Ogo, H. Hiramatsu, K. Nomura, H. Yanagi, T. Kamiya, M. Hirano, and H. Hosono. *Appl. Phys. Lett.*, 93:032113, 2008.
 - ¹¹ H. Hosono, Y. Ogo, H. Yanagi, and T. Kamiya. *Electrochem. Solid-State Lett.*, 14:H13, 2011.
 - ¹² A. A. Bolzan, C. Fong, B. J. Kennedy, and C. J. Howard. *Acta Crystallogr. Sect. B: Struct. Sci.*, 53:373, 1997.
 - ¹³ J. Pannetier and G. Denes. *Acta Crystallogr. B*, 36:2763, 1980.
 - ¹⁴ S. Cahen, N. David, J. M. Fiorani, A. Maïre, and M. Vilasi. *Thermochimica Acta*, 403(2):275, 2003, and references therein.
 - ¹⁵ J. Zhao, R. Tan, W. Shen, Y. Yang, Y. Guo, J. Li, Z. Zhou, J. Jian, and W. Song. *Mater. Lett.*, 84:94, 2012.
 - ¹⁶ C. Wang, G. Du, K. Stahl, H. Huang, Y. Zhong, and J. Z. Jiang. *J. Phys. Chem. C*, 116:4000, 2012.
 - ¹⁷ H. Spandau and E. J. Kohlmeyer. *Z. Anorg. Chem.*, 254:65, 1947.
 - ¹⁸ P. Spinedi and F. Gauzzi. *Ann. di Chim.*, 47:1305, 1957.
 - ¹⁹ A. Ditte. *Ann. Chimie Physique*, page 145, 1882.
 - ²⁰ O. M. Berengue, R. A. Simon, J. Chiquito, C. J. Dalmaschio, E. R. Leite, H. A. Guerreiro, and

- F. E. G. Guimarães. *J. Appl. Phys.*, 107:033717, 2010.
- ²¹ A. F. Holleman and E. Wiberg. *Lehrbuch der anorganischen Chemie*. Walter de Gruyter, 1995.
- ²² F. Lawson. *Nature*, 215:955, 1967.
- ²³ M. S. Moreno, G. Rigotti G. Punte, R. C. Mercader, A. D. Weisz, and M. A. Blesa. *Solid State Ionics*, 144:81, 2001.
- ²⁴ K. G. Bogatina D. N. Klushin, O. V. Nadinskaya. *J. Appl. Chem. USSR*, 32:284, 1959.
- ²⁵ M. Trömel G. Murken. *Z. Anorg. Allg. Chem.*, 397:117, 1973.
- ²⁶ C. Decroly and M. Ghodsi. *C. R. Acad. Sci.*, 261:2659, 1965.
- ²⁷ A. Seko, A. Togo, F. Oba, and I. Tanaka. *Phys. Rev. Lett.*, 100:045702, 2008.
- ²⁸ M. A. Mäki-Jaskari and T. T. Rantala. *Modelling Simul. Mater. Sci. Eng*, 12:33, 2004.
- ²⁹ K. Govaerts, R. Saniz, B. Partoens, and D. Lamoen. *Phys. Rev. B*, 87:235210, 2013.
- ³⁰ G. Kresse and J. Furthmüller. *Comput. Mater. Sci.*, 6:15, 1996.
- ³¹ G. Kresse and J. Furthmüller. *Phys. Rev. B*, 54:11, 1996.
- ³² J. P. Perdew, K. Burke, and M. Ernzerhof. *Phys. Rev. Lett.*, 77:3865, 1996.
- ³³ J. Klimeš, D. R. Bowler, and A. Michaelides. *Phys. Rev. B*, 83:195131, 2011.
- ³⁴ J. Heyd, G. E. Scuseria, and M. Ernzerhof. *J. Chem. Phys.*, 118:8207, 2003.
- ³⁵ A. V. Krukau, O. A. Vydrov, A. F. Izmaylov, and G. E. Scuseria. *J. Chem. Phys.*, 125:224106, 2006.
- ³⁶ H. D. Monkhorst and J. D. Pack. *Phys. Rev. B*, 13:5188, 1976.
- ³⁷ M. Shishkin and G. Kresse. *Phys. Rev. B*, 75:235102, 2007.
- ³⁸ M. Shishkin and G. Kresse. *Phys. Rev. B*, 74:035101, 2006.
- ³⁹ S. Curtarolo, D. Morgan, and G. Ceder. *Calphad*, 29:163, 2005.
- ⁴⁰ A. Walsh and G. W. Watson. *J. Phys. Chem. B*, 109:18868, 2005.